Published Ahead of Print on March 15, 2022 as 10.1212/WNL.0000000000200148

OPEN

Neurology®

The most widely read and highly cited peer-reviewed neurology journal
The Official Journal of the American Academy of Neurology

AMERICAN ACADEMY OF NEUROLOGY®

Neurology Publish Ahead of Print
DOI: 10.1212/WNL.0000000000200148

Spatial-Temporal Patterns of Amyloid-β Accumulation: A Subtype and Stage Inference Model Analysis

Author(s):
Lyduine E. Collij, PhD[1]; Gemma Salvadó, PhD[2,3]; Viktor Wottschel, PhD[1]; Sophie E Mastenbroek, MSc.[1]; Pierre Schoenmakers, BSc.[1]; Fiona Heeman, MSc.[1]; Leon Aksman, PhD[4]; Alle Meije Wink, PhD[1]; Bart N.M. Berckel, PhD, MD[1]; Wiesje M van de Flier, PhD[5,6]; Philip Scheltens, PhD, MD[5]; Pieter Jelle Visser, PhD, MD[5]; Frederik Barkhof, PhD, MD[1,7]; Sven Haller, PhD, MD[8,9,10,11]; Juan Domingo Gispert, PhD[2,3,12]; Isadora Lopes Alves, PhD[1] on behalf of for the Alzheimer's Disease Neuroimaging Initiative; for the ALFA study

Corresponding Author:
Lyduine E. Collij, l.collij@amsterdamumc.nl

Affiliation Information for All Authors: 1. Amsterdam UMC, Vrije Universiteit Amsterdam, Department of Radiology and Nuclear Medicine, De Boelelaan 1117, Amsterdam, Netherlands; 2. Barcelonaβeta Brain Research Center (BBRC), Pasqual Maragall Foundation, Barcelona, Spain; 3. IMIM (Hospital del Mar Medical Research Institute), Barcelona, Spain; 4. Stevens Neuroimaging and Informatics Institute, Keck School of Medicine, University of Southern California, Los Angeles, California, United States; 5. Alzheimer Center and Department of Neurology, Amsterdam UMC, Vrije Universiteit Amsterdam, De Boelelaan 1117, Amsterdam, Netherlands; 6. Amsterdam UMC, Vrije Universiteit Amsterdam, Department of Epidemiology & Data science, De Boelelaan 1117, Amsterdam, Netherlands; 7. Centre for Medical Image Computing, and Queen Square Institute of Neurology, UCL, United Kingdom; 8. Faculty of Medicine of the University of Geneva, Geneva, Switzerland; 9. CIMC - Centre d'Imagerie Médicale de Cornavin, Place de Cornavin 18, 1201 Genève 1201 Genève; 10. Department of Surgical Sciences, Radiology, Uppsala University, Uppsala, Sweden; 11. Department of Radiology, Beijing Tiantan Hospital, Capital Medical University, Beijing, 100070, P. R. China; 12. Centro de Investigación Biomédica en Red de Bioingeniería, Biomateriales y Nanomedicina (CIBER-BBN), Madrid, Spain.

Equal Author Contribution:

Contributions:
Lyduine E. Collij: Drafting/revision of the manuscript for content, including medical writing for content; Major role in the acquisition of data; Study concept or design; Analysis or intepretation of data
Gemma Salvadó: Drafting/revision of the manuscript for content, including medical writing for content; Major role in the acquisition of data; Study concept or design; Analysis or intepretation of data
Viktor Wottschel: Drafting/revision of the manuscript for content, including medical writing for content; Major role in the acquisition of data; Study concept or design
Sophie E Mastenbroek: Drafting/revision of the manuscript for content, including medical writing for content; Study concept or design; Analysis or intepretation of data
Pierre Schoenmakers: Drafting/revision of the manuscript for content, including medical writing for content; Analysis or intepretation of data
Fiona Heeman: Drafting/revision of the manuscript for content, including medical writing for content; Analysis or intepretation of data
Leon Aksman: Drafting/revision of the manuscript for content, including medical writing for content; Study concept or design; Analysis or intepretation of data
Alle Meije Wink: Drafting/revision of the manuscript for content, including medical writing for content; Study concept or design
Bart N.M. Berckel: Drafting/revision of the manuscript for content, including medical writing for content; Analysis or intepretation of data
Wiesje M van de Flier: Drafting/revision of the manuscript for content, including medical writing for content; Study concept or design; Analysis or intepretation of data
Philip Scheltens: Drafting/revision of the manuscript for content, including medical writing for content; Study concept or design
Pieter Jelle Visser: Drafting/revision of the manuscript for content, including medical writing for content
Frederik Barkhof: Drafting/revision of the manuscript for content, including medical writing for content; Analysis or intepretation of data
Sven Haller: Drafting/revision of the manuscript for content, including medical writing for content; Study concept or design; Analysis or intepretation of data
Juan Domingo Gispert: Drafting/revision of the manuscript for content, including medical writing for content; Major role in Sthe acquisition of data; Study concept or design; Analysis or intepretation of data

Isadora Lopes Alves: Drafting/revision of the manuscript for content, including medical writing for content; Major role in the acquisition of data; Study concept or design; Analysis or intepretation of data

Figure Count:
4

Table Count:
2

Search Terms:
[26] Alzheimer's disease, [122] PET, Amyloid

Acknowledgment:
Data used in precreation of this article were obtained from the Alzheimer's Disease Neuroimaging Initiative (ADNI) database (adni.loni.usc.edu). As such, the investigators within the ADNI contributed to the design and implementation of ADNI and/or provided data but did not participate in analysis or writing of this report. The data used in this publication is part of the ALFA (ALzheimer and FAmilies) study. The authors would like to express their most sincere gratitude to the ALFA project participants, without whom this research would have not been possible. Collaborators of the ALFA study are: Annabella Beteta, Anna Brugulat, Raffaele Cacciaglia, Alba CaÃ±as, Carme Deulofeu, Irene Cumplido, Ruth Dominguez, Maria Emilio, Karine Fauria, Sherezade Fuentes, Laura Hernandez, Gema Huesa, Jordi Huguet, Paula Marne, Tania MenchÃ³n, Albina Polo, Sandra Pradas, Blanca Rodriguez-Fernandez, Aleix Sala-Vila, Gonzalo SÃ¡nchez-Benavides, Gemma SalvadÃ³, Anna Soteras, and Marc Vilanova.

Study Funding:
The project leading to this paper has received funding from the Innovative Medicines Initiative 2 Joint Undertaking under grant agreement No 115952. This Joint Undertaking receives the support from the European Union's Horizon 2020 research and innovation programme and EFPIA. This communication reflects the views of the authors and neither IMI nor the European Union and EFPIA are liable for any use that may be made of the information contained herein. ALFA study received funding from "la Caixa" Foundation (ID 100010434), under agreement LCF/PR/GN17/50300004 and the Alzheimer's Association and an international anonymous charity foundation through the TriBEKa Imaging Platform project (TriBEKa-17-519007). Additional support has been received from the Universities and Research Secretariat, Ministry of Business and Knowledge of the Catalan Government under the grant no. 2017-SGR-892. JDG is supported by the Spanish Ministry of Science and Innovation (RYC-2013-13054) and the Agencia Estatal de Investigación Proyectos de I+D+i RETOS INVESTIGACIÓN (RTI2018-102261-B-I00).

Disclosures:
L. E. Collij reports no disclosures relevant to the manuscript; G. SalvadÃ³ reports no disclosures relevant to the manuscript; V. Wottschel reports no disclosures relevant to the manuscript; Sophie E. Mastenbroek reports no disclosures relevant to the manuscript; P. Schoenmakers reports no disclosures relevant to the manuscript; F. Heeman reports no disclosures relevant to the manuscript; L. Aksman reports no disclosures relevant to the manuscript; A. M. Wink reports no disclosures relevant to the manuscript; B. N. M. van Berckel reports no disclosures relevant to the manuscript; W. M. van der Flier reports no disclosures relevant to the manuscript; P. Scheltens received grants from GE Healthcare, Piramal, and Merck, paid to his institution; he has received speaker's fees paid to the institution Alzheimer Center, VU University Medical Center, Lilly, GE

Healthcare, and Roche; P. J. Visser has served as member of the advisory board of Roche Diagnostics. Dr Visser received nonfinancial support from GE Healthcare, research support from Biogen and grants from Bristol-Myers Squibb, EU/EFPIA Innovative Medicines Initiative Joint Undertaking, EU Joint ProgrammeÂ–Neurodegenerative Disease Research (JPND and ZonMw; F. Barkhof received payment and honoraria from Bayer Genzyme, Biogen-Idec, TEVA, Merck, Novartis, Roche, IXICO Ltd, GeNeuro, and Apitope Ltd for consulting; payment from the IXICOLtd, and MedScape for educational presentations; research support via grants from EU/EFPIA Innovative Medicines Initiative Joint Undertaking (AMYPAD consortium), EuroPOND (H2020), UK MS Society, Dutch MS Society, PICTURE (IMDI-NWO), NIHR UCLH Biomedical Research Centre (BRC), ECTRIMS-MAGNIMS; S. Haller is a member of the EPAD Imaging SAG, consultant for Spineart, consultant for WYSS, and speaker for GE Healthcare; J. D. Gispert has received speaker's fees from Biogen and Philips. In addition he.holds a Â‘RamÃ³n y CajalÂ’ fellowship (RYC-2013-13054), has received research support from the EU/EFPIA Innovative Medicines Initiative Joint Undertaking AMYPAD grant agreement nÂ° 115952, and from Ministerio de Ciencia y Universidades (grant agreement RTI2018-102261); I. Lopes Alves reports no disclosures relevant to the manuscript.

Handling Editor Statement:

ABSTRACT

Background and objectives: Currently, amyloid-β (Aβ) staging models assume a single spatial-temporal progression of amyloid accumulation. We assessed evidence for Aβ accumulation subtypes by applying the data-driven Subtype and Stage Inference (SuStaIn) model to amyloid-PET data.

Methods: Amyloid-PET data of 3010 subjects were pooled from 6 cohorts (ALFA+, EMIF-AD, ABIDE, OASIS, and ADNI). Standardized uptake value ratios (SUVr) were calculated for 17 regions. We applied the SuStaIn algorithm to identify consistent subtypes in the pooled dataset based on the cross-validation information criterion (CVIC) and the most probable subtype/stage classification per scan. The effect of demographics and risk factors on subtype assignment was assessed using multinomial logistic regression.

Results: Participants were mostly cognitively unimpaired (*N*=1890, 62.8%), had a mean age of 68.72 (*SD*=9.1), 42.1% was *APOE*-ε4 carrier, and 51.8% was female. While a one-subtype model recovered the traditional amyloid accumulation trajectory, SuStaIn identified an optimal of three subtypes, referred to as Frontal, Parietal, and Occipital based on the first regions to show abnormality. Of the 788 (26.2%) with strong subtype assignment (>50% probability), the majority was assigned to Frontal (*N*=415, 52.5%), followed by Parietal (*N*=199, 25.3%), and Occipital subtypes (*N*=175, 22.2%).

Significant differences across subtypes included distinct proportions of *APOE*-ε4 carriers (Frontal:61.8%, Parietal:57.1%, Occipital:49.4%), subjects with dementia (Frontal:19.7%, Parietal:19.1%, Occipital:31.0%) and lower age for the Parietal subtype (Frontal/Occipital:72.1y, Parietal:69.3y). Higher amyloid (Centiloid) and CSF p-tau burden was observed for the Frontal subtype, while Parietal and Occipital did not differ. At follow-up, most subjects (81.1%) maintained baseline subtype assignment and 25.6% progressed to a later stage.

Discussion: While a one-trajectory model recovers the established pattern of amyloid accumulation, SuStaIn determined that three subtypes were optimal, showing distinct associations to AD risk factors. Nonetheless, further analyses to determine clinical utility is warranted.

INTRODUCTION

Positron emission tomography (PET) imaging is one of the main currently available tools to study amyloid pathology *in vivo*. The technique makes use of amyloid-β (Aβ) radiotracers validated against neuropathology [1-3]. In comparison with other Aβ biomarkers such as cerebrospinal fluid (CSF) or plasma, PET imaging provides spatial-temporal information [4], which may be of particular interest for Alzheimer's disease (AD) research and clinical trials.

Since the first proposal of a population-based neuropathological progression scheme by Braak & Braak in 1991 [5], multiple amyloid PET studies proposed similar frameworks that would allow the staging of an individual's biomarker along a spectrum of pathological burden [6-9]. These approaches have demonstrated high applicability at the population level, and indicate that determining the extent of amyloid pathology can be used to better characterize prognosis and risk of cognitive decline [7-9]. However, these models have invariably relied on the assumption that the path to AD dementia-like levels of Aβ is the same across individuals, disregarding variability in the data that could point to distinct trajectories of amyloid accumulation. On the other hand, most studies aimed at identifying disease subtypes assume subjects to be at a common disease stage (e.g. dementia) for valid comparison [10], which is especially challenging in a sporadic and long-term disease processes such as AD. Therefore, while both approaches are useful, stage-only models do not disentangle potential subtypes, and subtype-only models do not account for distinct stages across individuals, hampering the identification of the simultaneous effect of subtypes and stages on disease presentation and risk assessment [11].

Recently, a data-driven method has been developed to jointly resolve both stages and subtypes from heterogeneous cross-sectional data, namely the Subtype and Stage Inference (SuStaIn) model [11]. This algorithm was previously applied to uncover patterns of brain atrophy in AD, showing an improved prediction of clinical conversion compared to stage- or subtype-only models [11]. More recent work identified four distinct spatio-temporal phenotypes of tau accumulation, which were associated with different clinical profiles and longitudinal cognitive outcomes, suggesting the value of such models

for improving individualized prognosis and clinical care [13]. In the context of amyloid, previous descriptions of a homogeneous spatial-temporal progression of amyloid pathology were not in full agreement[4], and staging models' success could be attributed to a reduced spatial resolution (i.e. small number of stages covering large portions of the brain)[8, 9]. Therefore, it is possible that an underlying heterogeneity in amyloid spatial-temporal progression remains unresolved.

To determine whether there is evidence for patterns of cerebral Aβ accumulation, we applied the SuStaIn model to pooled amyloid-PET data from five cohorts. These included observational cohorts and open-access data repositories with mostly cognitively unimpaired individuals, and clinical populations with different levels of cognitive impairment. We first assessed whether subtypes of progression are statistically preferred to the common assumption of a universal trajectory. We then described possible subtype differences with respect to main demographics and risk factors. Finally, we validated the observed subtypes in a longitudinal sub-set of data.

METHODS

Cohorts

From five cohorts, all participants with available amyloid PET scans of sufficient quality for quantification were retrospectively included (**Table 1**). [^{18}F]Flutemetamol scans of 358 cognitively unimpaired (CU) subjects from the Alzheimer's and Family (ALFA) cohort of the Barcelonaβeta Brain Research Center [14] and 190 CU subjects from the Innovative Medicine Initiative European Medical Information Framework for AD (EMIF-AD) [15] were included. [^{18}F]Florbetaben scans of 350 memory clinic patients from the Alzheimer's biomarkers in daily practice (ABIDE) study were included [16]. From the Open Access Series of Imaging Studies (OASIS)-3 dataset [17], 572 [^{11}C]Pittsburgh compound B (PiB) and 360 [^{18}F]florbetapir scans of CU subjects were obtained. Finally, 1180 subjects scanned with [^{18}F]florbetapir were included from the Alzheimer's Disease Neuroimaging Initiative (ADNI) database. The ADNI study was launched in 2003 as a public-private partnership, led by principal investigator Michael W. Weiner, MD. The primary goal of ADNI is to test whether serial MRI, PET, other biological markers, and clinical and neuropsychological assessment can be combined to measure the progression of mild cognitive impairment (MCI) and early AD.

In total, the complete data-set available for this study consisted of amyloid PET imaging data from 3010 subjects (1890 CU, 648 Cognitively Impaired (CI), 445 Dementia, and 27 with missing diagnosis at time of baseline PET). Subjects that were labeled as CI had a clinical diagnosis of mild cognitive impairment or a Clinical Dementia Rating of 0.5 in the absence of a clinical diagnosis. In addition, from cohorts where longitudinal PET imaging was available (ADNI and OASIS), we selected those for whom a second scan was performed ≥4 years after baseline (*N*=519).

Standard Protocol Approvals, Registrations, and Patient Consents

The protocol, patient information, consent form, and other relevant study documentation were approved by the Ethics Committees or Institutional Review Boards of each site before study

initiation. The studies were performed in accordance with the Declaration of Helsinki and consistent with Good Clinical Practice. Before enrollment, all patients provided written informed consent.

Image acquisition and processing

[^{18}F]Flutemetamol scans from the ALFA cohort consisted of four frames (4x5 minutes) acquired 90-110 minutes post-injection (p.i.). Images were checked for motion, and PET and accompanying structural T1-weighted MR images were warped into MNI space using SPM12. [^{18}F]flutemetamol EMIF-AD scans were acquired using a dual-time-window protocol [18] (0-30 minutes p.i., 60 minute break, 90-110 minutes p.i.), but only the late frames (90-110 min p.i.) were used for this work [19]. [^{18}F]florbetaben scans from ABIDE were processed as described previously, with static scans consisting of four frames (4x5 minutes) acquired 90-110 minutes p.i. [19]. All EMIF-AD and ABIDE images were checked for motion and accompanying structural T1-weighted MR images were co-registered to PET using the Vinci software (Max Planck Institute for Neurological Research, Cologne, Germany) and then warped into MNI using SPM12. [^{18}F]Florbetapir (50-70 minutes p.i.) and [^{11}C]PiB (30-60 minutes p.i.) data from the OASIS platform were processed with FreeSurfer and the PET Unified Pipeline [20]. Finally, [^{18}F]florbetapir PET scans from ADNI consisted of four frames (4x5 minutes), acquired 50-70 minutes p.i. and were processed using FreeSurfer.

PET quantification

For all cohorts, standard uptake value ratios (SUVr) relative to the cerebellar gray matter were available for all Desikan-Killiany atlas regions [21]. For the purposes of this work, a set of 17 regions of interest (ROI) was constructed by volume-weighted averaging of anatomically adjacent regions. The final 17 regions were the anterior, posterior and isthmus cingulate, medial and lateral orbitofrontal, precuneus, inferior, middle and superior frontal, supramarginal, insula and lingual gyrus, the lateral parietal lobe (superior and inferior parietal), lateral temporal lobe (middle, transverse and superior temporal, superior temporal sulcus, and temporal pole), basal temporal lobe (fusiform and inferior

temporal), occipital lobe (lateral occipital, cuneus and pericalcarine), and striatum (caudate and putamen).

In order to pool regional data across cohorts and tracers, SUVr values were standardized to z-scores. The z-scoring transformation was cohort-, radiotracer- and region-specific and the reference groups consisted of CU subjects of each study. We applied Gaussian Mixture Modeling to the regional data of each reference group to select the mean and standard deviation of the left ('normal') Gaussian curve. These refined regional estimates were then used for z-scoring the regional SUVr values (**eFigure 1**).

In addition, standardized quantification of global amyloid burden was obtained using the Centiloid (CL) scale [22]. PET scans from the ALFA, EMIF-AD, and ABIDE studies were processed by Barcelonaβeta Brain Research Center (BBRC) using a validated standard Centiloid pipeline [23]. Centiloid values were directly obtained from the OASIS-3 and ADNI databases. As per standard guidelines, the reference region used for CL was the whole cerebellum for all data [22].

Subtype and Stage Inference (SuStaIn) Model

In this work, the Mixture SuStaIn implementation in PySuStaIn, cloned from the master branch of on 30 October 2020, was used with Python 3.7. SuStaIn is a probabilistic machine learning algorithm that can characterize the heterogeneity of disease by inferring both patterns of disease progression (subtypes) and an individual's disease stage (i.e. degree of progression within a subtype) from cross-sectional data. Importantly, the number of SuStaIn stages is defined by the number of biomarkers (in our case ROIs) provided to the model. The model uses a data likelihood based on how far a biomarker measurement deviates from normality to group events based on their associated z-score (e.g. one, two or three standard deviations away from control population mean) for each biomarker. However, in cases where the control population displays little abnormality (such as the case in our work, where amyloid load in the reference group will be low), the resulting z-scores in patients can become too large in comparison. Instead, it is more sensible to use two distributions, one to describe

the control population and a separate one to describe patients' measurements, therefore defining an event as a biomarker (in our case regional SUVr of the 17 pre-defined ROIs) going from normal to abnormal (as in the event-based model; EBM [12, 24]).

The SuStaIn model fitting consists of an iterative procedure that simultaneously optimizes subtype event sequences and subtype classification for a pre-selected number of subtypes. Model out-of-sample likelihoods across 10-folds were used to calculate the cross-validation information criterion (CVIC) per model. The CVIC is a measure of how well the model fits the test data, similar to the Akaike information criterion, but with less penalty on model complexity[25]. A complete mathematical description of the SuStaIn algorithm can be found in Young and colleagues [11]. The number of subtypes was iteratively increased, and the model chosen for further analysis was selected based on the CVIC. In particular, we repeated the cross-validation analysis 20 times to exclude spurious findings and picked the subtype model such that the CVIC was lowest or, in cases where the CVIC was very similar, had the lower model complexity (i.e. fewer subtypes).

Statistical Analyses

Statistical analyses were performed using Statistical Package for the Social Sciences (SPSS) version 26, and significance was set at $p<0.05$.

Optimal model fit

The SuStaIn model was constructed based on the full baseline data-set (N=3010) and the optimal number of subtypes was tested by iteratively increasing the number of selected subtypes until the lowest CVIC value was reached. In addition, Spearman rank correlation analyses were used to assess the agreement between the regional ordering of a one-trajectory model (i.e. 'one' subtype, as per previously proposed staging models) and that of each of the subtypes determined by the optimal model. Rank correlations between each subtypes were also determined.

Subtype analyses

Overall differences between subtypes were assessed independently of stage. First, subjects classified as stage 0 were labeled as 'no subtype' and excluded for analyses. For subjects assigned to stage ≥1, only those with a strong probability (>50%) of assignment to a subtype were included. A multinomial logistic regression (MLR) was used to determine the effect of demographics and risk factors on subtype assignment, such as age, cohort representation, proportion of males/females, *APOE*-ε4 and *APOE*-ε2 carriers, Mini-Mental State Examination (MMSE) scores, and diagnostic groups. Next, two separate MLRs were used to determine the relationship between subtypes and biomarkers of AD pathology (amyloid and p-tau), corrected for the variables above. In addition to z-scored CSF p-tau, the first model included Centiloid as a marker for amyloid pathology, while the second model included z-scored CSF $A\beta_{42}$. CSF values were z-scored based on the mean and standard deviation from the GMM derived normal curve of each cohort. CSF was available for 1522 subjects (ABIDE: 241 (15.8%), ADNI: 858 (56.4%), ALFA+: 303 (19.9%), EMIF-AD: 120 (7.9%)).

Longitudinal validation

The optimal SuStaIn model derived from the baseline data was subsequently applied to the sub-set (*N*=591) of available longitudinal amyloid PET scans. Descriptive statistics were used to determine subtype stability (proportion of subjects classified as the same subtype at follow-up) and stage progression (proportion of subjects with lower, same or higher stage at follow-up). In addition, a MLR was used to assess whether annualized rates of change in Centiloid were different between subtypes, accounting for all significant covariates and baseline amyloid burden.

Data Availability

The data that support the findings of this study can be made available upon request with the study-specific principal investigator (i.e. ABIDE, EMIF-AD, ALFA) or are openly available (i.e. ADNI & OASIS open-source databases).

RESULTS

Main demographics are shown in **Table 1**. Across cohorts, subjects had a mean age of 68.72 ± 9.06, 51.8% were female. Most subjects were cognitively unimpaired (*N*=1890, 62.4%), MMSE=27.88 ± 2.93 and the proportion of *APOE*-ε4 carriers was relatively high (42.1%).

Identified subtypes of amyloid accumulation

The optimal model fit identified three different subtypes according to the CVIC (**eFigures 2–3**). The three subtypes are referred to as Frontal, Parietal, and Occipital in the remainder of this study according to the earliest regions to become abnormal in each of them.

The Frontal subtype identified the first abnormalities in amyloid PET signal in the medial orbitofrontal region, progressing from the anterior to the posterior parts of the brain, and culminating with the involvement of the striatum and the occipital lobe. Similarly, the Parietal subtype also identified the striatum and occipital lobe as the last to become abnormal, while first regions to display abnormality were the posterior cingulate and the precuneus with the intermediate spatial-temporal progression evolving from posterior to anterior regions. Finally, the Occipital subtype displayed an inverse overall ordering, beginning in the occipital and temporal-parietal lobes, progressing to frontal regions and ending in the striatum (**Figure 1A, eFigure 4**).

In comparison, the regional ordering from a one-trajectory model closely resembled previously proposed staging models, with a medial frontal and precuneal start of amyloid accumulation, expanding throughout the cortex, and ending with the occipital cortex and striatum (**Figure 1B**). This regional ordering was strongly and positively correlated with the regional ordering of the Frontal (ρ=0.90, p<0.001), and the Parietal (ρ=0.89, p<0.001) subtypes, but not with the Occipital subtype (ρ= -0.01, p=0.96; **eFigure 5**). When comparing subtypes, the regional ordering of the Frontal and Parietal was positively correlated (ρ=0.74, p<0.001), while Occipital subtype regional ordering did not

significantly correlate with the Frontal (ρ=-0.18, p=.50) or Parietal subtypes (ρ=-0.4, p<0.88; **eFigure 6**).

Subtype assignment

Across the complete baseline data-set (N=3010), the majority of scans either showed fully normal (stage 0: N=1810, 60.1%) or widespread abnormal (stage 17: N=282, 9.4%) Aβ levels across all brain regions, which challenged accurate subtype assignment (**Figure 2**). Therefore, only cases with a strong subtype assignment probability (>50% probability) across stages higher than 0 were selected for subsequent subtype analyses (N=788, 26.2%). Within the 788 subjects with strong subtype assignment, the majority (N=415, 52.5%) was assigned to the Frontal, followed by the Parietal (N=199, 25.3%), and Occipital subtypes (N=175, 22.2%). This distribution was present within each cohort, with the exception of ABIDE (N=101) where the majority of subjects (N=46, 45.5%) were assigned to the Parietal subtype instead (χ^2=70.31, p<0.001, **Figure 3A, eTable 1**).

Subtype differences

Demographics per subtype can be found in **Table 2.** The proportion of males/females was similar between subtypes. Subjects assigned to the Parietal subtype were younger compared to the Frontal (β=0.05, p<0.001) and Occipital (β=0.04, p=0.005). While MMSE scores did not differ between subtypes, diagnostic groups were differentially represented, with Occipital displaying a higher proportion of subjects with dementia than the other two (vs Frontal: β=0.84, p<0.001; vs Parietal: β=0.63, p=0.02, **Figure 3B**). The proportion of carriers across subtypes was similar for the ε2 allele (6.6-7.9%), while ε4 carriership differed, with the highest percentage of *APOE*-ε4 carriers observed in the Frontal subtype (vs Parietal: β=-0.43, p=0.02; vs Occipital: β=-0.79, p<0.001; **Figure 3C**).

With respect to the biomarkers of AD pathology, MLR analyses (N=430) corrected for the variables above showed significantly higher amyloid burden as expressed in CL levels for the Frontal subtype compared to the Parietal (β=-0.02, p=0.002) and Occipital (β=-0.01, p=0.02), but no differences for

CSF $A\beta_{42}$**Figure 3D/E**). CSF p-tau levels were also significantly higher for the Frontal subtype compared to Parietal (CL model: β=-0.19, *p*=0.006; CSF $A\beta_{42}$ model: β=-0.25, *p*<0.001) and Occipital (CL model: β=-0.10, *p*=0.11; CSF $A\beta_{42}$ model: β=-0.14, *p*=0.03), while Parietal and Occipital did not differ (**Figure 3F**).

Longitudinal validation

A total of 519 (ADNI *N*=376 [72.4%]; OASIS *N*=143 [27.6%]) subjects had available longitudinal amyloid PET at least 4 years after baseline available (*M*=5.5±1.2 [4.0 – 9.6] years). Mean follow-up time was longer for OASIS (*M*=6.2±1.4 [4.0 – 9.6] years) compared to ADNI (*M*=5.2±1.0 [4.0 – 9.4] years, *F*=71.0, *p*<0.001). Subjects with longitudinal PET data had highly similar demographics compared to the full cohort, with most participants being CU as baseline (*N*=320, 61.7%), had a mean MMSE score of 28.72 (*SD*=1.61), an average age of 70.0 years (*SD*=9.01), and 51.3% was female.

The longitudinal validation was performed across the entire sample (even if the baseline probability of subtype assignment was lower than 50%). In the complete longitudinal sample, the majority of subjects were assigned to 'no subtype' (i.e. stage 0) at baseline (*N*=381, 73.4%), followed by Frontal subtype (*N*=86, 16.6%), Parietal (*N*=47, 9.1%) and Occipital (*N*=5, 1.0%).

Subtype stability

In the entire longitudinal sample, 421 (81.1%) subjects were stable in subtype assignment; 322 remained stage 0 i.e. 'no subtype', 65 from the Frontal, and 34 from the Parietal subtype. In contrast, 98 (18.9%) subjects changed subtype assignment at follow-up ('no subtype'=59, Frontal=21, Parietal=13, and Occipital=5 at baseline). From those, Frontal mostly changed to Parietal and vice-versa (F→P: 76.2%, *N*=16 and F→0: 23.8%, *N*=5| P→F: 76.9%, *N*=10 and P→O: 7.7%, *N*=1), while all Occipital subjects (*N*=4) changed subtype, and mostly to Parietal (O→F: 20.0%, *N*=1 and O→P: 60.0%, *N*=3, **Figure 4A**). The most common "change in subtype" occurred in subjects who started in stage 0 (0→F: 66.1%, *N*=39, 0→P: 30.5%, *N*=18, 0→O: 3.4%, *N*=2, **Figure 4B**).

Amyloid accumulation

When we evaluated staging, we found that 69.0% (*N*=358) remained stable, 25.6% (*N*=133) progressed to later stages, and 5.4% (*N*=28) of subjects regressed in stage at follow-up. This was independent of subtype stability. These changes in stage can also be observed using the Centiloid scale (**Figure 4C**). Yearly rates of change in Centiloid were different between subjects assigned to one of the three subtypes or 'no subtype' at baseline, even after accounting for syndromic diagnosis, cohort, *APOE*-ε4 carriership and baseline amyloid burden. More specifically, the longitudinal rates of change were lower for the 'no subtype' (vs Frontal: β=4.09 p<0.001; vs Parietal: β=4.23 p<0.001; vs Occipital: β=2.84 p=0.004) and slightly higher for Occipital subtype (vs Frontal: β=-0.08 p<0.001; vs Parietal: β=-0.07 p=0.03 ; vs no subtype: β=-0.35, p<0.001), but did not differ between the Frontal and Parietal subtypes.

DISCUSSION

In this work, applying the Subtype and Stage Inference (SuStaIn) model to a pooled data-set of >3000 PET scans provided support for the existence of 3 subtypes of topographical cortical amyloid accumulation, in contrast to the traditional assumption of single-trajectory models reported previously [4, 6, 8, 9]. The three subtypes are referred to as Frontal, Parietal, and Occipital based on the earliest regions to show abnormality. Of these, the Frontal subtype was most prevalent in our sample and was associated with a higher proportion of *APOE*-ε4 carriership and higher amyloid and tau burden, while the Parietal subtype was associated with younger age. The Occipital subtype showed a higher proportion of patients with dementia.

Previous models of amyloid accumulation in AD were based on the assumption of a universal trajectory of disease progression, consistently implicating the medial cortical regions early in the process of Aβ accumulation, followed by cortical association areas, and finally the late involvement of occipital and striatal regions [6-9]. This population-level ordering was also identified by SuStaIn when the model was set to recover one trajectory, which seems to correspond to an average of the most

common Frontal and Parietal subtypes (**eFigure 2**). We now extend on former studies, as SuStaIn was able to further resolve subtype-specific initial stages, identifying the orbitofrontal cortex and precuneus regions as the starting point of distinct subtypes. Further, we observed that the concomitant abnormality in those regions corresponded to an intermediate SuStaIn stage shared between the Frontal and Parietal subtypes instead (i.e. ~Stage 8, **Figure 1**). Importantly, the precuneus seems more strongly implicated in patients with early-onset AD [27]. In line, the Parietal subtype was more often observed in the ABIDE clinical cohort from the Alzheimercenter Amsterdam, a tertiary referral center specialized in dementia at a young age [16, 28].

In the absence of neuropathological confirmation, it is important to note that recent work on regional visual assessment of [^{18}F]flutemetamol PET images supports these results [29]. The expert visual assessment of almost 500 amyloid-PET images showed both the traditional joint and early involvement of the medial orbitofrontal cortex and precuneus, as well as a non-negligible proportion of cognitively unimpaired subjects displaying isolated amyloid burden, specifically in one of these regions [29]. Unfortunately, the occipital lobe is not part of the visual read guidelines of amyloid PET images [29], limiting the available information on the incidence of occipital uptake. Nonetheless, a subset of subjects in this previous report did show an relatively early involvement of temporal regions, especially together with parietal ones – a pattern that could reflect the first half of the Occipital subtype progression (up to ~stage 9, **Figure 1**).

Importantly, the identification of the Occipital subtype by SuStaIn is remarkably distinct from traditional reports of early amyloid deposition in AD. In fact, the occipital lobe is commonly assumed to only harbor amyloid pathology towards the end of the disease process [6, 8, 9]. Nonetheless, posterior or occipital uptake is often attributed to cerebral amyloid angiopathy (CAA), which most commonly affects this region and is a known risk factor for AD [30]. Under this hypothesis, the assignment of subjects to the Occipital subtype could suggest the identification of CAA as cerebral Aβ accumulation by SuStaIn. Nonetheless, there is neuropathological support for an alternative hypothesis, i.e. that the occipital signal actually reflects cortical amyloid pathology. More specifically,

Braak and Braak (1991) described basal occipital uptake as part of the first neuropathological stage in AD [5]. Also, (posterior) amyloid burden is observed in approximately 50% of patients with Lewy Body dementia (DLB), which is suggested to reflect AD co-pathology and is associated with a worse prognosis [31]. A post-hoc analysis of subtype classification in specifically the clinical ABIDE cohort provides further support of this observation, as the Occipital subtype was overrepresented in the DLB patient population (**eFigure 7**). To further determine the underlying pathology of this subtype, its relationship to (occipital-) micro bleeds (a symptom of CAA [30]) and different etiologies in patients with non-AD dementia should be investigated. Still, this over-representation of subjects with dementia in the Occipital subtype indicates that early amyloid-PET signal in the occipital lobe may harbor relevant prognostic information. As such, future AD research should consider the assessment of occipital regions, and future visual read guidelines could consider including the occipital lobe for the assessment of amyloid PET scans should these findings be confirmed.

Overall, subtype assignment might have the highest utility in the pre-dementia stages of AD, considering the main differences between the trajectories are apparent at the beginning of the process. Indeed, the highest probability of subtype assignment was observed in individuals at the early-to-intermediate stages of amyloid-PET abnormality (stages 6-7), while higher stages resulted in lower probability of assignment since subtypes merge into similar trajectories (**Figure 2**). Nonetheless, the earliest regions of each subtype still display higher amyloid at the late stages, indicating that subtypes can still be identified even beyond the amyloid saturation point. While this suggests that the subtypes are not merely ephemeral states, an important question is whether they have prognostic value, both in terms of differences in speed of amyloid accumulation as well as in terms of risk or speed of subsequent pathological progress and cognitive decline. Regarding the former, our longitudinal analyses already suggest the Frontal subtype to have lower amyloid accumulation rates compared to the other groups. However, these results must be interpreted with caution, as the sample size of both Parietal and Occipital subtypes were too small. Another possible impact of amyloid subtypes could be related to subsequent tau spread. While previous literature

suggests tau spread beyond the medial temporal lobe to only occur after sufficient amyloid deposition, it remains unclear whether and how the spatial distribution of amyloid further influences this event. In addition, recent work identified four subtypes of tau accumulation, further suggesting a possible interaction between amyloid and tau spatial-temporal trajectories[13]. In terms of cognition, the different proportions of clinical diagnostic groups (i.e. cognitively unimpaired, cognitively impaired and dementia) already indicate worse prognosis for the Occipital subtype. Nonetheless, clinical diagnosis is a relatively crude measure for overall cognitive performance, and further exploration of the severity and type of cognitive symptoms associated with each of the subtypes will be necessary to determine their clinical relevance. In addition, previous work has shown that the extent of amyloid burden as measured in CL units predicts the risk of global cognitive decline [32]. Future work should investigate whether additional information on amyloid accumulation subtype further improves risk stratification.

There are some methodological limitations to consider when interpreting the results of this work. First, while SuStaIn uses a cross-validation framework and the results are bootstrapped, one could argue we should have used a separate training- and test-set to validate the results. We opted not to do this, as the majority of subjects were cognitively normal and had no amyloid, thus the amount of data with variable amyloid burden was already limited. In addition, it should be noted that the majority of the data included in this work was previously used to describe a one-trajectory amyloid accumulation pattern, though implementing a different methodological approach [9]. Thus, the high agreement between the SuStaIn-identified one-trajectory model and some of the previous staging work is possibly partly due to the re-use of data. Second, while Centiloid units are generally used to pool PET data, we standardized regional SUVr using a z-scoring approach. This was done to account for not only tracer differences, but also for the differential signal distortion effects between medial and lateral regions (inherit to the PET metric) [4], which is not taken into account in the Centiloid approach [22]. Third, while our initial results suggest robust assignment over time (i.e. stable for 87.7% of subjects), only ADNI and OASIS-3 had available longitudinal PET imaging data, limiting our sample

sizes for longitudinal analyses, especially for the Occipital subtype. Finally, yearly rates of change in amyloid burden might be underestimated for the Occipital subtype, as the Centiloid mask does not include this region.

CONCLUSION

The SuStaIn model provides data-driven evidence for the existence of three spatio-temporal subtypes of cortical amyloid accumulation and opens possibilities for further exploration of the identified subtypes. The initial results indicate differences in their relation to AD risk factors as well as prognosis, and therefore suggest subtype assignment may have clinical relevance and/or could support individualized risk assessment. Future work should assess whether subtypes are associated with distinct cognitive profiles or risk of cognitive decline and investigate the possible underlying pathophysiology.

Table 1. Baseline demographics for each cohort

Tracer	[^{18}F]flutemetamol		[^{18}F]florbetaben			[^{11}C]PiB			[^{18}F]florbetapir							
Cohort	**ALFA (*N* = 358)**	**EMIF-AD (*N* = 190)**	**ABIDE (*N* = 350)**			**OASIS (*N* = 572)**			**OASIS (*N* = 360)**			**ADNI (*N* = 1180)**				**Total (*N*=3010)**
Diagnostic group	**CU**	**CU**	**CU (*N* = 126)**	**CI (*N* = 66)**	**Dementia (*N* = 158)**	**CU (*N* = 482)**	**CI (*N* = 32)**	**Dementia (*N* = 58)**	**CU (*N* = 304)**	**CI (*N* = 25)**	**Dementia (*N* = 31)**	**Missing (*N* = 27)**	**CU (*N* = 430)**	**CI (*N* = 525)**	**Dementia (*N* = 198)**	**CU=1890 / CI=648 / Dementia=445 / Missing=27**
Age (SD)	61.50 (4.64)	70.44 (7.55)	60.53 (7.80)	66.13 (7.09)	66.68 (7.34)	64.63 (9.32)	70.44 (8.35)	74.09 (8.21)	66.78 (8.51)	70.92 (6.30)	73.50 (6.84)	72.72 (9.84)	73.97 (6.78)	72.87 (7.96)	75.02 (7.75)	68.72 (9.06)
Sex (F)	220 (61.5%)	112 (58.9%)	54 (42.9%)	24 (36.4%)	65 (41.1%)	292 (60.6%)	18 (56.3%)	24 (41.4%)	163 (53.6%)	17 (68.0%)	19 (61.3%)	14 (51.9%)	233 (54.2%)	222 (42.3%)	82 (41.4%)	1559 (51.8%)
MMSE (SD)	29.18 (0.95)	28.99 (1.14)	27.77 (2.40)	26.94 (2.01)	23.12 (4.09)	29.13 (1.15)	27.97 (1.94)	23.77 (6.01)	29.04 (1.26)	28.56 (1.53)	24.45 (4.07)	26.00 (2.55)	29.06 (1.19)	28.02 (1.78)	22.49 (3.28)	27.88 (2.93)
***APOE*-ε4 carriership +**	198 (55.3%)	62 (33.3%)	49 (38.9%)	31 (47.0%)	83 (52.5%)	161 (33.5%)	15 (46.9%)	35 (60.3%)	101 (34.7%)	7 (30.4%)	23 (74.2%)	8 (36.4%)	124 (29.0%)	241 (45.9%)	129 (65.5%)	1267 (42.1%)
***APOE*-ε2 carriership +**	31 (8.7%)	17 (8.9%)	15 (11.9%)	9 (13.6%)	12 (7.6%)	81 (16.8%)	4 (12.5%)	6 (10.3%)	52 (17.9%)	3 (13.0%)	2 (6.5%)	1 (4.5%)	57 (13.3%)	52 (9.9%)	8 (4.1%)	350 (11.6%)
Centiloid (SD)	2.76 (17.02)	14.58 (23.02)	13.00 (26.53)	28.35 (32.36)	45.51 (45.15)	11.77 (26.70)	36.75 (43.74)	72.14 (42.55)	18.77 (32.06)	47.02 (59.19)	75.70 (42.30)	39.71 (39.32)	17.79 (27.89)	33.45 (35.89)	60.43 (35.33)	24.24 (35.75)
Aβ-positivity[$]	38 (10.6%)	40 (21.1%)	29 (23.0%)	29 (43.9%)	101 (63.9%)	90 (18.7%)	14 (43.8%)	49 (84.5%)	85 (28.0%)	13 (52.0%)	27 (87.1%)	15 (55.6%)	125 (29.1%)	275 (52.4%)	167 (84.3%)	1097 (36.4%)
CSF $A\beta_{42}$ (SD)	1309.38 (371.89)	892.28 (317.98)	1078.08 (283.21)	906.45 (319.25)	745.72 (298.79)	N/A			N/A			N/A	1246.92 (433.15)	1016.95 (431.53)	696.12 (338.48)	N/A
CSF P-Tau (SD)	16.44 (7.49)	76.34 (44.38)	53.98 (29.84)	65.75 (27.82)	70.90 (33.08)	N/A			N/A			N/A	22.13 (9.35)	26.60 (14.32)	36.71 (16.37)	N/A

CSF Essay	Elecsys	Adx Euroimmune	Innotest	N/A	N/A	Elecsys	

CU = cognitively unimpaired, which includes both controls and subjective cognitive decliners; CI = cognitively impaired, subjects either had a clinical diagnosis of mild cognitive impairment or a Clinical Dementia Rating of 0.5 (in the absence of a clinical diagnosis)

Dementia includes both AD or non-AD

[#] Subject carries at least 1 *APOE*-ε4 allele

[†] Subject carries at least 1 *APOE*-ε2 allele

[$] Aβ-positivity = CL>21

Table 2 . Baseline demographics for each subtype

Subtype	Frontal (*N* = 414)	Parietal (*N* =199)	Occipital (*N* = 175)
Diagnostic group (N)	Missing = 2 (0.5%) CU = 215 (51.9%) CI = 112 (27.1%) Dementia = 82 (19.8%)	Missing = 2 (1.0%) CU = 109 (54.8%) CI = 50 (25.1%) Dementia = 38 (19.1%)	Missing = 4 (2.3%) CU = 77 (44.0%) CI = 41 (23.4%) Dementia = 53 (30.3%)
Age (SD)	72.12 (8.14)	69.26 (9.61)	72.13 (8.07)
Sex (F)	196 (47.3%)	97 (43.7%)	85 (48.6%)
MMSE (SD)	27.35 (3.19)	27.40 (2.56)	26.56 (3.50)
APOE-ε4 carriership +[#]	264 (64.2%)	113 (57.7%)	86 (49.4%)
APOE-ε2 carriership +[†]	31 (7.5%)	13 (6.6%)	12 (6.9%)
Centiloid (SD)	50.73 (27.52)	36.71 (28.99)	40.65 (29.26)
z-scored CSF $A\beta_{42}$ (SD)	-2.45 (1.60)	-2.19 (1.78)	-2.38 (1.72)
z-scored CSF P-Tau (SD)	2.08 (2.501)	0.91 (2.03)	1.51 (2.03)

CU = cognitively unimpaired, which includes both controls and subjective cognitive decliners; CI = cognitively impaired, subjects either had a clinical diagnosis of mild cognitive impairment or a Clinical Dementia Rating of 0.5 (in the absence of a clinical diagnosis)

Dementia includes both AD or non-AD

[#] Subject carries at least 1 *APOE*-ε4 allele

[†] Subject carries at least 1 *APOE*-ε2 allele

FIGURE LEGENDS

Figure 1. In **(A)**, a representation of the final three subtypes as identified by SuStaIn, referred to as Frontal (top row), Parietal (middle row) and Occipital (bottom row), as in accordance to the earliest regions to become abnormal; in **(B)**, the same representation for a one-trajectory model across the data-set, which was not preferred against the three-subtype model.

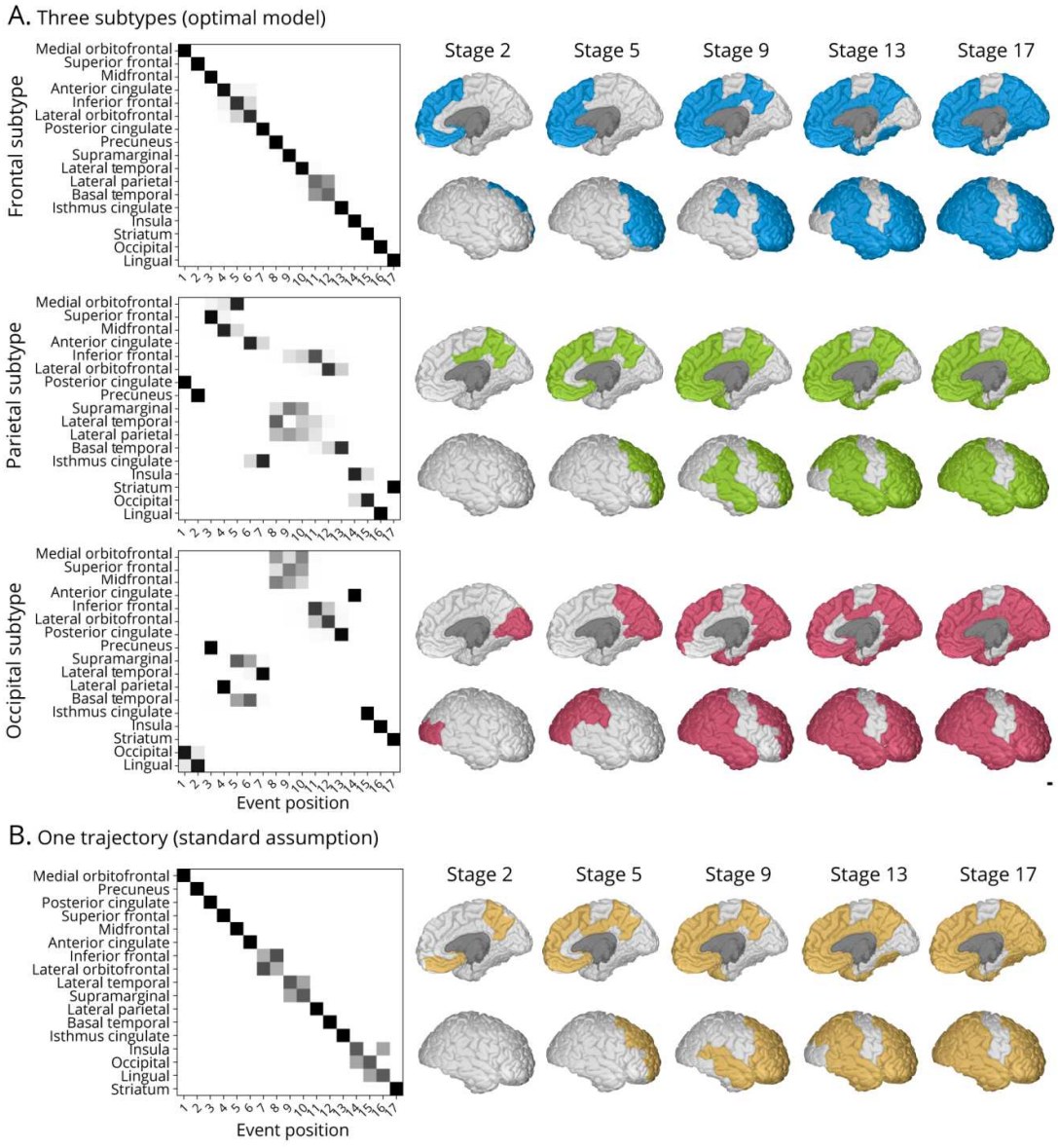

Figure 2. Subtype assignment probability against assigned stage

Boxplots shows the relationship between stage assignment on the x-axis against the probability of subtype assignment on the y-axis for the whole baseline data-set. The solid line represents the cut-off for high probability, i.e. >50%. It can be appreciated that subtype assignment probability is lowest for those subjects in stage 0 or 17, who present little least spatio-temporal information. Also, the highest probability assignment is observed for those subjects around 7, where the subtypes are most different from each other.

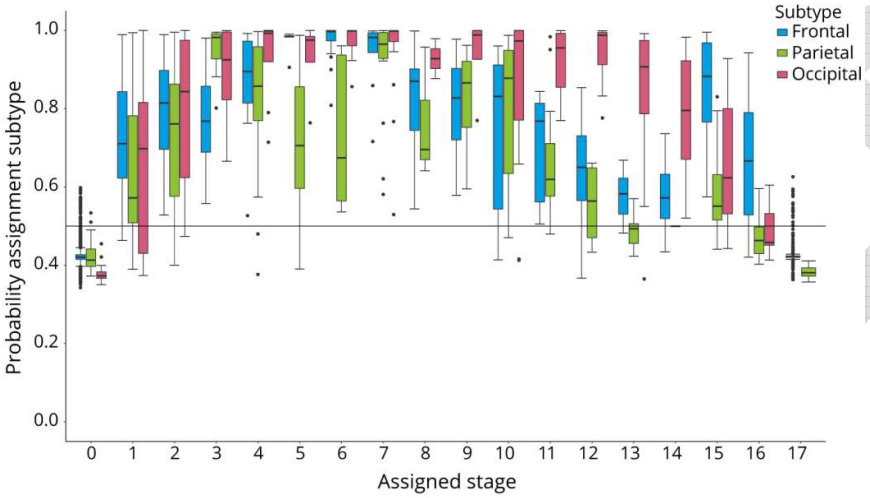

Figure 3. Cross-sectional relationships

For the 788 subjects with a strong subtype assignment (>50% probability) at baseline, differences in subtypes are shown for **A)** cohort and tracer representation, **B)** diagnostic groups, **C)** *APOE*-ε4 carriership, **D)** amyloid burden expressed in Centiloid units, **E)** amyloid burden in CSF $A\beta_{42}$, and **F)** CSF p-tau. Demographics and risk factors (**A-C**) were significantly different between the three subtypes. **D/F)** The Frontal subtype was associated with higher Centiloid and CSF p-tau values, **E)** though no differences were observed for CSF $A\beta_{42}$ between subtype .

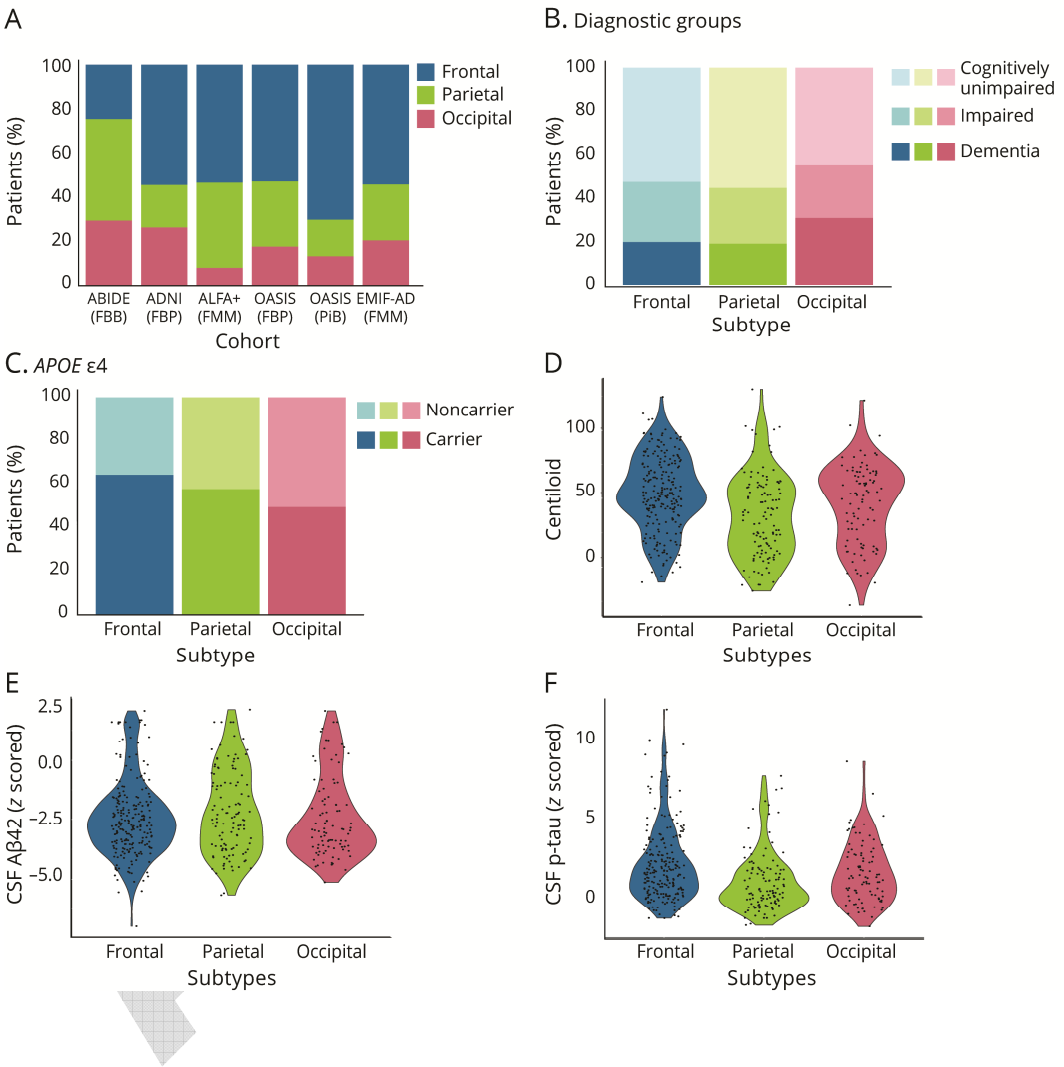

Figure 4. Longitudinal validation

In panel **A)**, the subtype assignment at baseline vs at follow-up is shown. Spaghetti plots illustrates the change in **B)** stage and **C)** Centiloid (CL) units per subtype as assigned at baseline. Lines are color coded to show changes in subtype assignment at follow-up. Overall, changes in stage are associated with changes in CL and yearly rates of change were lowest for the Frontal subtype.

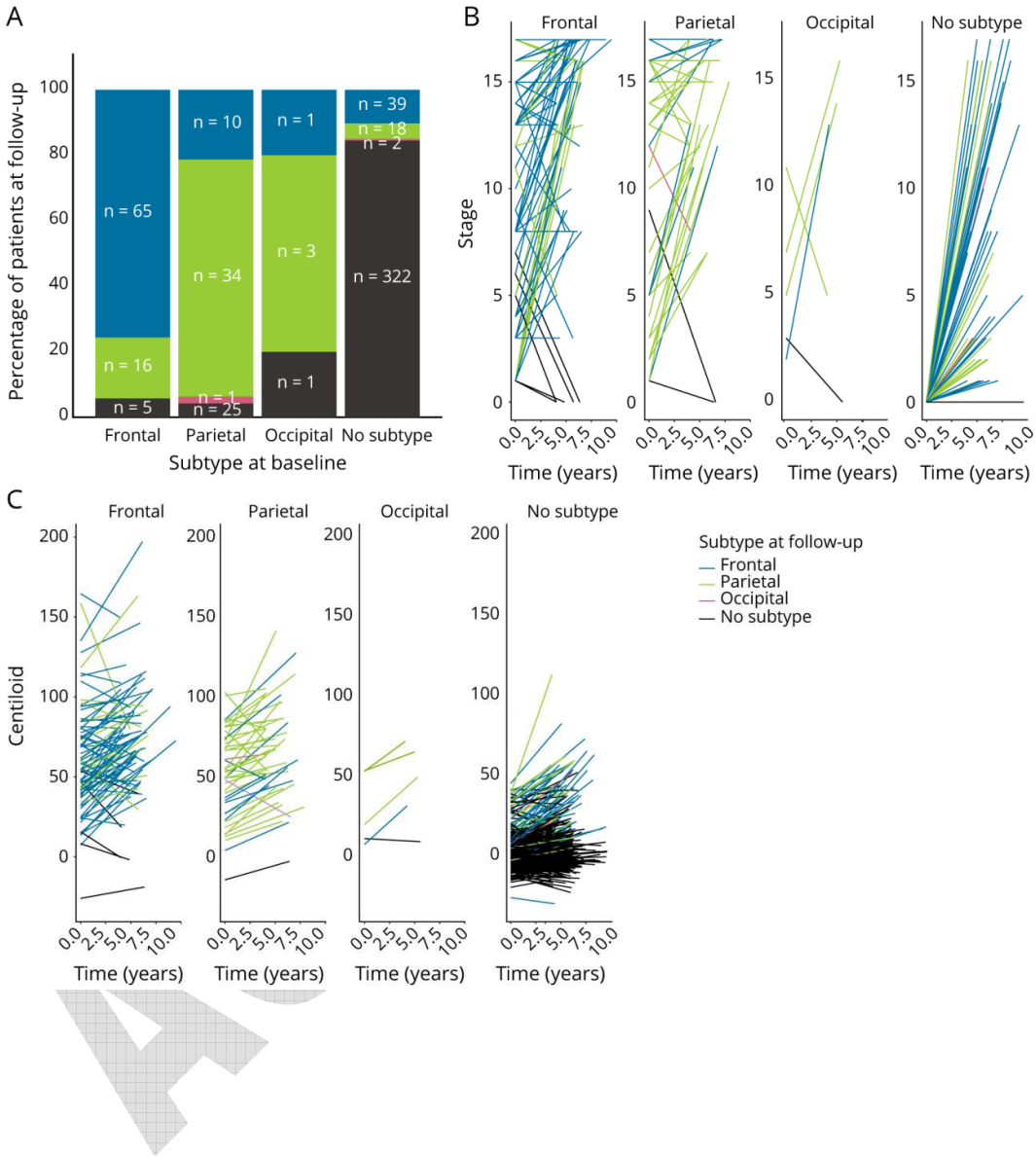

Appendix 1– Authors

Name	Location	Contribution
Lyduine E. Collij, PhD	Amsterdam UMC, VUmc, Amsterdam, NL	Literature search, design, data collection, analysis, interpretation, drafted manuscript
Gemma Salvadó, PhD	Barcelonaβeta Research Center, Barcelona, ES	Literature search, design, data collection, analysis, interpretation, drafted manuscript
Viktor Wottschel, PhD	Amsterdam UMC, VUmc, Amsterdam, NL	Design, analysis, interpretation, drafted manuscript, revised manuscript
Sophie E. Mastenbroek, MSc.	Amsterdam UMC, VUmc, Amsterdam, NL	Analyses, interpretation, drafted manuscript, revised manuscript
Pierre Schoenmakers, BSc.	Amsterdam UMC, VUmc, Amsterdam, NL	Data collection, analysis, revised manuscript
Fiona Heeman, MSc.	Amsterdam UMC, VUmc, Amsterdam, NL	Data collection, interpretation, revised manuscript
Leon M. Aksman, PhD	Stevens Neuroimaging and Informatics Institute, University of Southern California, Los Angeles, US.	Analysis, revised manuscript
Alle Meije Wink, PhD	Amsterdam UMC, VUmc, Amsterdam, NL	Interpretation, revised manuscript
Bart N.M. van Berckel, PhD	Amsterdam UMC, VUmc, Amsterdam, NL	Data collection, interpretation, revised manuscript
Wiesje M. van der Flier, PhD	Amsterdam UMC, VUmc, Amsterdam, NL	Data collection, analyses, interpretation, revised manuscript
Philip Scheltens, PhD	Amsterdam UMC, VUmc, Amsterdam, NL	Data collection, revised manuscript
Pieter Jelle Visser, PhD	Amsterdam UMC, VUmc, Amsterdam, NL	Data collection, revised manuscript
Frederik Barkhof, PhD	Amsterdam UMC, VUmc, Amsterdam, NL; University College London, London, UK	Data collection, interpretation, revised manuscript
Sven Haller, PhD	Faculty of Medicine of the University of Geneva, Geneva, Switzerland	Design, analyses, interpretation, revised manuscript
Juan Domingo Gispert, PhD	Barcelonaβeta Research Center, Barcelona, ES;	Design, data collection, analyses, interpretation, revised manuscript
Isadora Lopes Alves, PhD	Amsterdam UMC, VUmc, Amsterdam, NL	Literature search, design, analysis, interpretation, drafted manuscript

WNL-2022-200401_sup ---http://links.lww.com/WNL/B861

WNL-2022-200401_coinvestigator_appendix2 --http://links.lww.com/WNL/B862

WNL-2022-200401_coinvestigator_appendix3 --http://links.lww.com/WNL/B863

REFERENCES

1. Salloway S, Gamez JE, Singh U, et al. Performance of [(18)F]flutemetamol amyloid imaging against the neuritic plaque component of CERAD and the current (2012) NIA-AA recommendations for the neuropathologic diagnosis of Alzheimer's disease. *Alzheimers Dement (Amst)*. 2017;9:25-34. doi:10.1016/j.dadm.2017.06.001
2. Sabri O, Sabbagh MN, Seibyl J, et al. Florbetaben PET imaging to detect amyloid beta plaques in Alzheimer's disease: phase 3 study. *Alzheimers Dement*. Aug 2015;11(8):964-74. doi:10.1016/j.jalz.2015.02.004
3. Clark CM, Schneider JA, Bedell BJ, et al. Use of florbetapir-PET for imaging β-amyloid pathology. *Jama*. 2011;305(3):275-283.
4. Fantoni E, Collij L, Alves IL, Buckley C, Farrar G. The spatial-temporal ordering of amyloid pathology and opportunities for PET imaging. *J Nucl Med*. Dec 13 2019;doi:10.2967/jnumed.119.235879
5. Braak H, Braak E. Neuropathological stageing of Alzheimer-related changes. *Acta Neuropathol*. 1991;82(4):239-59.
6. Grothe MJ, Barthel H, Sepulcre J, et al. In vivo staging of regional amyloid deposition. *Neurology*. Nov 14 2017;89(20):2031-2038. doi:10.1212/WNL.0000000000004643
7. Hanseeuw BJ, Betensky RA, Mormino EC, et al. PET staging of amyloidosis using striatum. *Alzheimers Dement*. May 21 2018;doi:10.1016/j.jalz.2018.04.011
8. Mattsson N, Palmqvist S, Stomrud E, Vogel J, Hansson O. Staging β-amyloid pathology with amyloid positron emission tomography. *JAMA neurology*. 2019;76(11):1319-1329.
9. Collij LE, Heeman F, Salvado G, et al. Multitracer model for staging cortical amyloid deposition using PET imaging. *Neurology*. Sep 15 2020;95(11):e1538-e1553. doi:10.1212/WNL.0000000000010256
10. Ossenkoppele R, Schonhaut DR, Scholl M, et al. Tau PET patterns mirror clinical and neuroanatomical variability in Alzheimer's disease. *Brain*. May 2016;139(Pt 5):1551-67. doi:10.1093/brain/aww027
11. Young AL, Marinescu RV, Oxtoby NP, et al. Uncovering the heterogeneity and temporal complexity of neurodegenerative diseases with Subtype and Stage Inference. *Nat Commun*. Oct 15 2018;9(1):4273. doi:10.1038/s41467-018-05892-0
12. Young AL, Oxtoby NP, Daga P, et al. A data-driven model of biomarker changes in sporadic Alzheimer's disease. *Brain*. Sep 2014;137(Pt 9):2564-77. doi:10.1093/brain/awu176
13. Vogel JW, Young AL, Oxtoby NP, et al. Four distinct trajectories of tau deposition identified in Alzheimer's disease. *Nat Med*. 2021/04/29 2021;doi:10.1038/s41591-021-01309-6

14. Molinuevo JL, Gramunt N, Gispert JD, et al. The ALFA project: A research platform to identify early pathophysiological features of Alzheimer's disease. *Alzheimers Dement (N Y)*. Jun 2016;2(2):82-92. doi:10.1016/j.trci.2016.02.003
15. Konijnenberg E, Carter SF, Ten Kate M, et al. The EMIF-AD PreclinAD study: study design and baseline cohort overview. *Alzheimers Res Ther*. Aug 4 2018;10(1):75. doi:10.1186/s13195-018-0406-7 (http://www.emif.eu/emif-ad-2/)
16. de Wilde A, van Maurik IS, Kunneman M, et al. Alzheimer's biomarkers in daily practice (ABIDE) project: Rationale and design. *Alzheimers Dement (Amst)*. 2017;6:143-151. doi:10.1016/j.dadm.2017.01.003
17. LAMontagne PJ KS, Lauren W, Xiong C, Grant EA, Moulder KL, Morris JC, Bezinger TLS, Marcus DS. OASIS-3: Longitudinal Neuroimaging, Clinical, and Cognitivel Dataset for Normal Aging and Alzheimer's Disease. *AAIC 2018 poster presentation*. 2018;14(7):P1097. doi:https://doi.org/10.1016/j.jalz.2018.06.1439 (https://www.oasis-brains.org/)
18. Heeman F, Yaqub M, Lopes Alves I, et al. Optimized dual-time-window protocols for quantitative [(18)F]flutemetamol and [(18)F]florbetaben PET studies. *EJNMMI Res*. Mar 27 2019;9(1):32. doi:10.1186/s13550-019-0499-4
19. Collij L, Konijnenberg E, Reimand J, et al. Assessing Amyloid Pathology in Cognitively Normal Subjects using [(18)F]Flutemetamol PET: Comparing Visual Reads and Quantitative Methods. *J Nucl Med*. Oct 12 2018;doi:10.2967/jnumed.118.211532
20. Su Y, D'Angelo GM, Vlassenko AG, et al. Quantitative analysis of PiB-PET with FreeSurfer ROIs. *PLoS One*. 2013;8(11):e73377. doi:10.1371/journal.pone.0073377 (https://github.com/ysu001/PUP)
21. Desikan RS, Segonne F, Fischl B, et al. An automated labeling system for subdividing the human cerebral cortex on MRI scans into gyral based regions of interest. *Neuroimage*. Jul 1 2006;31(3):968-80. doi:10.1016/j.neuroimage.2006.01.021
22. Klunk WE, Koeppe RA, Price JC, et al. The Centiloid Project: standardizing quantitative amyloid plaque estimation by PET. *Alzheimers Dement*. Jan 2015;11(1):1-15 e1-4. doi:10.1016/j.jalz.2014.07.003
23. Salvado G, Molinuevo JL, Brugulat-Serrat A, et al. Centiloid cut-off values for optimal agreement between PET and CSF core AD biomarkers. *Alzheimers Res Ther*. Mar 21 2019;11(1):27. doi:10.1186/s13195-019-0478-z
24. Fonteijn HM, Modat M, Clarkson MJ, et al. An event-based model for disease progression and its application in familial Alzheimer's disease and Huntington's disease. *Neuroimage*. Apr 15 2012;60(3):1880-9. doi:10.1016/j.neuroimage.2012.01.062
25. Reiss PT, Huang L, Cavanaugh JE, Roy AK. Resampling-based information criteria for best-subset regression. *Annals of the Institute of Statistical Mathematics*. 2012;64(6):1161-1186.
26. Jagust W. Imaging the evolution and pathophysiology of Alzheimer disease. *Nat Rev Neurosci*. Nov 2018;19(11):687-700. doi:10.1038/s41583-018-0067-3
27. Ossenkoppele R, Zwan MD, Tolboom N, et al. Amyloid burden and metabolic function in early-onset Alzheimer's disease: parietal lobe involvement. *Brain*. Jul 2012;135(Pt 7):2115-25. doi:10.1093/brain/aws113
28. van der Flier WM, Scheltens P. Amsterdam Dementia Cohort: Performing Research to Optimize Care. *J Alzheimers Dis*. 2018;62(3):1091-1111. doi:10.3233/JAD-170850
29. Collij LE, Salvado G, Shekari M, et al. Visual assessment of [(18)F]flutemetamol PET images can detect early amyloid pathology and grade its extent. *Eur J Nucl Med Mol Imaging*. Feb 22 2021;doi:10.1007/s00259-020-05174-2

30. Charidimou A, Farid K, Tsai HH, Tsai LK, Yen RF, Baron JC. Amyloid-PET burden and regional distribution in cerebral amyloid angiopathy: a systematic review and meta-analysis of biomarker performance. *J Neurol Neurosurg Psychiatry*. Apr 2018;89(4):410-417. doi:10.1136/jnnp-2017-316851
31. Chetelat G, Arbizu J, Barthel H, et al. Amyloid-PET and (18)F-FDG-PET in the diagnostic investigation of Alzheimer's disease and other dementias. *Lancet Neurol*. Nov 2020;19(11):951-962. doi:10.1016/S1474-4422(20)30314-8
32. van der Kall LM, Truong T, Burnham SC, et al. Association of beta-amyloid level, clinical progression and longitudinal cognitive change in normal older individuals. *Neurology*. Nov 12 2020;doi:10.1212/WNL.0000000000011222
33. Scheltens P, De Strooper B, Kivipelto M, et al. Alzheimer's disease. *Lancet*. Mar 2 2021;doi:10.1016/S0140-6736(20)32205-4
34. Mila-Aloma M, Salvado G, Gispert JD, et al. Amyloid beta, tau, synaptic, neurodegeneration, and glial biomarkers in the preclinical stage of the Alzheimer's continuum. *Alzheimers Dement*. Oct 2020;16(10):1358-1371. doi:10.1002/alz.12131
35. Palhaugen L, Sudre CH, Tecelao S, et al. Brain amyloid and vascular risk are related to distinct white matter hyperintensity patterns. *J Cereb Blood Flow Metab*. Sep 21 2020:271678X20957604. doi:10.1177/0271678X20957604
36. Dicks E, van der Flier WM, Scheltens P, Barkhof F, Tijms BM, Alzheimer's Disease Neuroimaging I. Single-subject gray matter networks predict future cortical atrophy in preclinical Alzheimer's disease. *Neurobiol Aging*. Oct 2020;94:71-80. doi:10.1016/j.neurobiolaging.2020.05.008

Spatial-Temporal Patterns of Amyloid-β Accumulation: A Subtype and Stage Inference Model Analysis

Lyduine E. Collij, Gemma Salvadó, Viktor Wottschel, et al.

Neurology published online March 15, 2022
DOI 10.1212/WNL.0000000000200148